

# Optical properties of poly[2-methoxy-5-(3',7'-dimethyloctyloxy)-1,4-phenylenevinylene] light-emitting polymer solutions: effects of molarities and solvents

Bayram Gündüz<sup>1</sup>

Received: 22 September 2014 / Revised: 2 June 2015 / Accepted: 13 July 2015 /  
Published online: 26 July 2015  
© Springer-Verlag Berlin Heidelberg 2015

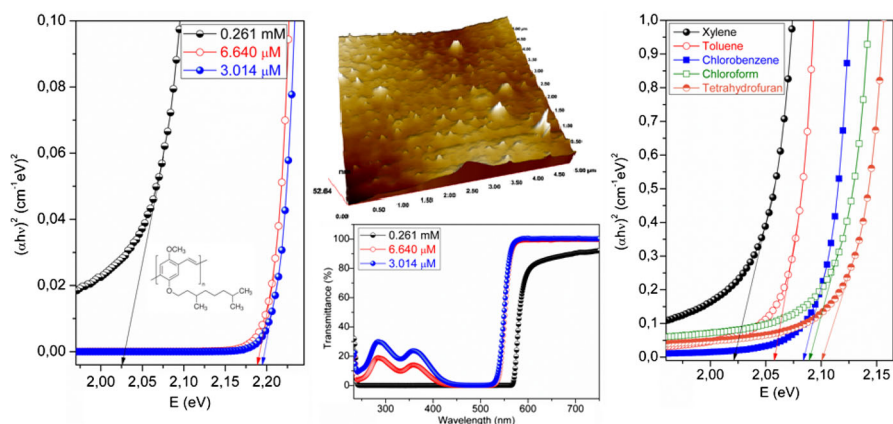
**Abstract** The optical properties of the solutions of the MDMO-PPV light-emitting polymer were investigated. The maximum mass extinction coefficient values of the solutions of the MDMO-PPV for 6.640 and 3.014  $\mu\text{M}$  were found to be 20.874 and 42.009  $\text{L g}^{-1} \text{cm}^{-1}$ , respectively. The absorption band edge values of the solutions of the MDMO-PPV shifted from 2.149 to 1.987 eV with increasing molarity. To obtain lower  $E_g$  values (2.020, 2.057, 2.083, 2.088 and 2.103 eV, respectively) of the MDMO-PPV can be preferred xylene, toluene, chlorobenzene, chloroform and tetrahydrofuran solvents, respectively. The  $E_g$  of the solution of the MDMO-PPV was decreased with molarities and solvents. The refractive index values of the MDMO-PPV were controlled with various solvents. The optical parameters such as single oscillator energy, dispersion energy,  $M_{-1}$ ,  $M_{-3}$  moments, optical oscillator strengths, linear static refractive index, optical linear susceptibility, third-order nonlinear susceptibility and nonlinear refractive index were calculated using Wemple–DiDomenico equation. The highest contrast was obtained with xylene, while the lowest contrast was obtained with chlorobenzene. The MDMO-PPV can be used in the fabrication of the metal–semiconductor contacts due to low optical band gap and suitable optical parameters. Also, the surface morphology properties of the MDMO-PPV polymer film were investigated.

---

✉ Bayram Gündüz  
bgunduz83@hotmail.com; b.gunduz@alparslan.edu.tr

<sup>1</sup> Department of Science Education, Faculty of Education, Muş Alparslan University, Muş 49250, Turkey

## Graphical abstract



**Keywords** MDMO-PPV · Molar/mass extinction coefficient · Single oscillator model

## Introduction

Conjugated polymers (CPs) are known as organic semiconductors with electronic properties and they have a wide application in electronic technology [1–6]. The polymers and especially CPs have been extensively used in electronic and optoelectronic device applications [7] such as organic field-effect transistors (OFETs), phototransistors, organic solar cells (OSCs), organic light-emitting diodes (OLEDs), sensors, lasers and electronic circuits due to simplified fabrication process of devices and their easy processing, unique processability from solution [8]. The CPs represent a novel class of semiconductors, which combine the optical and electronic properties of semiconductors with the processing advantages and mechanical properties of polymers [9]. These materials have shown potential for photovoltaic and photodetector applications due to their advantages of high absorption coefficient [4], flexibility, low cost, their high photoluminescence efficiency and low charged impurity.

Poly(p-phenylenevinylene) (PPV) and its derivatives are attractive class of materials for use in polymer light-emitting diode (PLED) application due to good device performance and their efficient electroluminescence (EL) [9]. Soluble PPV derivatives have high fluorescence and excellent solubility in common organic solvents [9]. Poly[2-methoxy-5-(3',7'-dimethyloctyloxy)-1,4-phenylenevinylene] (MDMO-PPV) light-emitting polymer (LEP) is completely soluble in common organic solvents such as dichloromethane (DCM), tetrahydrofuran (THF), toluene and chloroform and it is fluoresce bright orange color under UV light [9]. MDMO-PPV is a soluble conjugated polymer and it is the important donor-type polymer [10] in the fabrication of bulk-heterojunction photovoltaic cells and MDMO-PPV commonly used in the fabrication of the PLEDs.

The nonlinear optical properties such as optical absorption [12–14] have shown high potential [15] for device applications in far-infrared laser amplifiers [16], photo-detectors [17], and high-speed electro-optical modulators [18]. The extinction coefficients, including mass extinction coefficient ( $\alpha$ ) and molar extinction coefficient ( $\epsilon$ ), are parameters to define the absorbance intensity at a given wavelength per mass density (g) or molar concentration (mol), respectively [19]. It can be determined by using the Beer–Lambert law,  $Abs = \epsilon cl$ , where  $Abs$  is the absorbance which can be obtained using a UV–Vis absorbance spectrometer, and  $l$  is the optical path length [20].

Solvent affects on organic reactivity and absorption spectra have been studied for more than a century [21]. It is well known that the photo-physical behavior of a dissolved dye depends on the nature of its environment [21], that is, the shape, intensity, and maximum absorption wavelength of the absorption band of dye in solution depend strongly on the solvent–solute interactions and solvent nature [22]. This effect is closely related to the nature and degree of dye–solvent interactions [23]. Solvents influence on the optical and electrical properties of the materials.

Furthermore, some scientists made several researches on some optical properties of the MDMO-PPV film. Quist et al. [24] reported a MDMO-PPV with an absorption coefficient ( $\alpha$ ) value of  $1.3 \times 10^7 \text{ m}^{-1}$  at  $\lambda = 500 \text{ nm}$ . Omer [25] reported thin films of a conjugated polymer MDMO-PPV prepared from chloroform, 1,2 dichlorobenzene and toluene solutions by spin-coating technique on quartz substrates. He [25] reported MDMO-PPV thin films spin-coated from chloroform, 1,2 dichlorobenzene and toluene solvents with an absorption maximum peak ( $\lambda_{\text{max}}$ ) values of 491, 502 and 501 nm, and an optical band gap values of 2.15, 2.10 and 2.12 eV, respectively. Veenstra et al. [26] reported a MDMO-PPV with a long wavelength absorption maxima value of 518 nm in the spectra. Hoppe and Sariciftci [8] reported most conjugated polymers with the optical band gap values of around 2 eV. They [8] reported a MDMO-PPV thin film with a maximum absorption coefficient value of about  $2.0 \times 10^5 \text{ cm}^{-1}$ . Kim and Ryu [27] reported a MDMO-PPV with the highest occupied molecular orbital (HOMO) value of 5.33 eV and the lowest unoccupied molecular orbital (LUMO) value of 2.97 eV. Saxena et al. [28] reported the solution of MDMO-PPV polymer in chloroform with a peak value of emission spectra of 592 nm. It was not found any report in the literature about the optical properties of the solutions of the liquid-crystalline polymer MDMO-PPV for different molarities and solvents. This solution technique for investigation of the optical properties of the soluble materials has some advantages such as low cost and high accurate results.

Omer [25] also reported a thin film of a conjugated polymer MDMO-PPV fabricated from 1,2 dichlorobenzene and toluene with the area roughness values of 6.99 and 22.66 nm and the average height values of 28.51 and 68.85 nm, respectively. No report was found in the literature about the surface roughness parameters of the only MDMO-PPV polymer film such as roughness average ( $S_a$ ), root mean square roughness ( $S_q$ ), surface skewness ( $S_{sk}$ ) and surface kurtosis ( $S_{ku}$ ). Similarly, it was not found any report about the morphology of the cross section and height histograms of the MDMO-PPV polymer film.

In this study, the optical properties of the solutions of the MDMO-PPV polymer were investigated in detail. The optical measurements were conducted on a Shimadzu model UV-1800 Spectrophotometer. The aim of this study is to investigate the effects of the molarities on the optical parameters such as molar extinction coefficient, mass extinction coefficient, average transmittance, absorb wavelength, absorption band edge, optical band gap, real and imaginary parts of the dielectric constant, real and imaginary parts of conductivity. The optical band gap of the solution of the MDMO-PPV polymer was decreased with molarities and solvents. The optical parameters based on refractive index were calculated using Wemple–DiDomenico equation. Another aim of the study is to investigate the surface morphology properties of the MDMO-PPV light-emitting polymer film by high-performance atomic force microscopy (AFM). The surface roughness parameters of the MDMO-PPV film such as roughness average (Sa), root mean square roughness (Sq), surface skewness (Ssk) and surface kurtosis (Sku) were obtained. Also, I reported the morphology of the cross section (wall) and height histograms of the MDMO-PPV film by AFM.

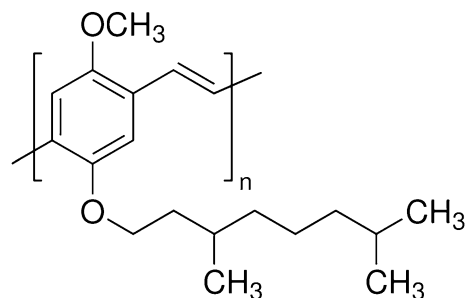
## Experimental

Poly[2-methoxy-5-(3',7'-dimethyloctyloxy)-1,4-phenylenevinylene] (MDMO-PPV) light-emitting polymer (LEP) and solvents, which are xylene, toluene, chlorobenzene, chloroform and tetrahydrofuran (THF) used in this study were purchased from Sigma-Aldrich Co. The chemical structure of the light-emitting polymer MDMO-PPV is shown in Fig. 1. This section has been occurred in three stages. In the first stage, the solutions of the MDMO-PPV polymer for different molarities and solvents were prepared. In the second stage, optical measurements of the solutions of the MDMO-PPV polymer for different molarities and solvents were recorded and in the last stage, the MDMO-PPV film for surface morphology properties was prepared.

### Preparation of the MDMO-PPV polymer solutions

To investigate the effects on the optical properties of the molarity and solvents, the MDMO-PPV polymer was weighed with a AND-GR-200 Series Analytical Balance

**Fig. 1** The chemical structure of the light-emitting polymer MDMO-PPV



for 0.261 mM, 6.640 and 3.014  $\mu\text{M}$  molarities in chloroform solvent and for xylene, toluene, chlorobenzene, chloroform and tetrahydrofuran solvents at 0.217 mM molarity. Then, these weighed MDMO-PPV polymers for different molarities and solvents were homogeneously dissolved in 8 mL volume of chloroform solvent and in 8 mL volume of xylene, toluene, chlorobenzene, chloroform and tetrahydrofuran solvents, respectively. Finally, the solutions of the MDMO-PPV polymer were filtered through PTFE membrane filter to obtain the best results of the optical measurements.

### **The optical measurements of the solutions of the MDMO-PPV polymer for different molarities and solvents**

The cylindrical cuvettes (Hellma QS-100) of 3.5 mL volume and 10 mm optical path length for all the solutions of the MDMO-PPV polymer were used. The optical measurements of the solutions of the MDMO-PPV polymer for different molarities and solvents were recorded by a Shimadzu model UV-1800 Spectrophotometer in the wavelength 1100–190 nm at room temperature.

### **Preparation of the MDMO-PPV film for surface morphology**

To prepare the MDMO-PPV film, the MDMO-PPV polymer was weighed with a AND-GR-200 Series Analytical Balance to prepare the solutions at 0.217 mM for surface morphology studies, then it was dissolved homogeneously in 5 mL volume of chloroform and was filtered through PTFE membrane filter to obtain the best film. Ultimately, the solution of the filtered MDMO-PPV polymer was coated on cleaned microscopy glass. After the coating, the film was dried at 70 °C for 15 min to evaporate the solvent and remove organic residuals. Surface morphology of the MDMO-PPV polymer film was investigated by high-performance atomic force microscopy (hpAFM, NanoMagnetics Instruments Co.) with PPP-XYNCHR type Cantilever at dynamic mode.

## **Results and discussion**

### **The optical properties of the solutions of the MDMO-PPV polymer for different molarities**

The absorbance (Abs) spectra of the solutions of the MDMO-PPV polymer were taken to investigate their optical properties for 0.261 mM, 6.640 and 3.014  $\mu\text{M}$  in chloroform solvent and the plot of the Abs vs. wavelength is shown in Fig. 2. As seen in Fig. 2, the absorbance values of the solutions of the MDMO-PPV polymer exist in the near ultraviolet (200–380 nm) and visible region (380–780 nm). This shows that the near ultraviolet and visible regions are very important regions for the light-emitting polymer MDMO-PPV. As seen in Fig. 2, the uncertainty, which results from high molarity in the absorbance values of the solution of the MDMO-PPV for 0.261 mM in the range of about 250 and 560 nm has disappeared with

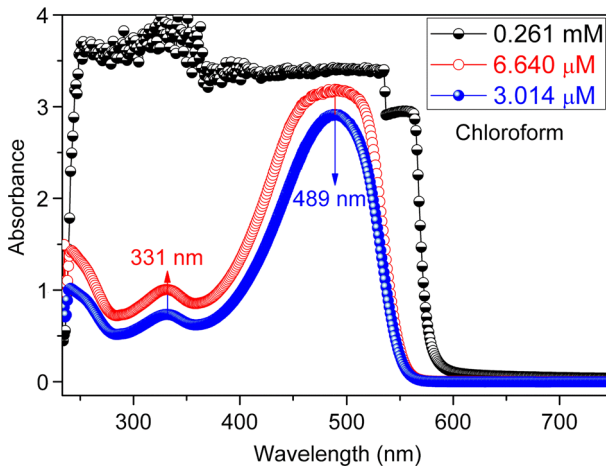


**Fig. 2** The plot of the absorbance vs. wavelength of the solutions of the MDMO-PPV polymer for 0.261 mM, 6.640 and 3.014  $\mu\text{M}$  in chloroform solvent

decreasing molarity. As seen in Fig. 2, the absorbance values of the MDMO-PPV polymer decrease with decreasing molarity and there is a peak both in the near ultraviolet and the visible region. The maximum absorption wavelength ( $\lambda_{\text{max}}$ ) of the solutions of the MDMO-PPV polymer for 6.640  $\mu\text{M}$  and 3.014  $\mu\text{M}$  was found to be 489 nm. The  $\lambda_{\text{max}}$  value (489 nm) of the solutions of the MDMO-PPV polymer in chloroform is smaller than the value (491 nm) of the MDMO-PPV thin films spin-coated from chloroform in the literature [25]. The  $\text{Abs}_{\text{max}}$  value of the solution of the MDMO-PPV polymer was obtained in the visible region and the  $\text{Abs}_{\text{max}}$  values at  $\lambda_{\text{max}}$  of the solutions of the MDMO-PPV polymer for 6.640  $\mu\text{M}$  and 3.014  $\mu\text{M}$  were found to be 3.188 and 2.912, respectively. The  $\text{Abs}_{\text{max}}$  values at  $\lambda_{\text{max}}$  (331 nm) value of the peak in the near ultraviolet region for 6.640  $\mu\text{M}$  and 3.014  $\mu\text{M}$  were found to be 1.006 and 0.733, respectively. It is observed that the  $\text{Abs}_{\text{max}}$  value of the solution of the MDMO-PPV polymer can be decreased with decreasing molarity. Finally, as seen in Fig. 2, the absorbance values of the solutions of the MDMO-PPV polymer sharply decrease after  $\lambda_{\text{max}}$  value (at 489 nm). In this study, the orange color of the MDMO-PPV polymer is emitted at about 598 nm (see Fig. 3) for 0.261 mM, while the yellow color of the MDMO-PPV polymer is emitted at about 580 nm (see Fig. 3) for 3.014  $\mu\text{M}$ . This attributes to color of the high and low molarities of the solutions of the MDMO-PPV polymer. The value (592 nm) [28] of emission spectra of polymer (MDMO-PPV) solution in chloroform in the literature is lower and higher than the values (598 and 580 nm, respectively) of emission spectra of the orange and yellow color of the MDMO-PPV polymer, respectively. These results attribute to difference of molarities of the solutions of the MDMO-PPV polymer. This situation probably is originated from high molarity of the solutions of the MDMO-PPV polymer in this study.

The molar extinction coefficient ( $\epsilon$ ) being an significant intrinsic parameter and reliable values of the  $\epsilon$  parameter for solutions are required in many engineering,

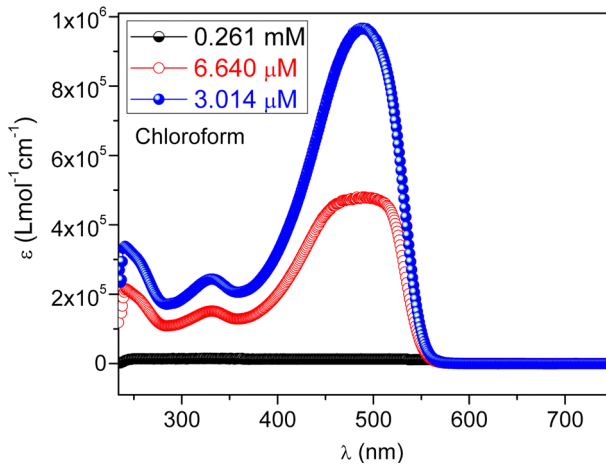


**Fig. 3** The molar extinction coefficient ( $\epsilon$ ) plot vs.  $\lambda$  of the solutions of the MDMO-PPV polymer for 0.261 mM, 6.640 and 3.014  $\mu\text{M}$  in chloroform solvent

scientific and chemical disciplines involving photo interactions [29]. The  $\epsilon$  values of the solutions of the MDMO-PPV polymer can be determined with an equation known as the Beer–Lambert law [20],

$$\epsilon = \frac{\text{Abs}}{cl} \quad (1)$$

where Abs is the actual absorption,  $l$  is the optical path length, and  $c$  is the molar concentration of the used cuvettes. The  $\epsilon$  values of the solutions of the MDMO-PPV polymer were calculated from Eq. (1). The  $\epsilon$  plot vs.  $\lambda$  of the solutions of the MDMO-PPV polymer for 0.261 mM, 6.640 and 3.014  $\mu\text{M}$  is shown in Fig. 3. As seen in Fig. 3, the molar extinction coefficient of the MDMO-PPV polymer increases with decreasing molarity. The high  $\epsilon$  value is very important to increase the device photocurrent density and conversion efficiency [30] and to have good light-harvesting ability and a higher short-circuit current density [31]. The maximum molar extinction coefficient ( $\epsilon_{\text{max}}$ ) values at  $\lambda_{\text{max}}$  value (489 nm) of the solutions of the MDMO-PPV polymer for 6.640 and 3.014  $\mu\text{M}$  were found to be  $4.801 \times 10^5$  and  $9.662 \times 10^5$   $\text{L mol}^{-1} \text{cm}^{-1}$ , respectively.

The mass extinction coefficients ( $\alpha_{\text{mass}}$ ) can be calculated by [19],

$$\alpha_{\text{mass}} = \frac{\epsilon}{M_A} \quad (2)$$

where  $M_A$  is the molecular mass of the material, which is the average 23,000 g/mol [32] of the light-emitting polymer MDMO-PPV. The maximum mass extinction coefficient ( $\alpha_{\text{mass-max}}$ ) values at  $\epsilon_{\text{max}}$  values ( $4.801 \times 10^5$  and  $9.662 \times 10^5$   $\text{L mol}^{-1} \text{cm}^{-1}$ , respectively) of the solutions of the MDMO-PPV polymer for 6.640 and 3.014  $\mu\text{M}$  were found to be 20.874 and 42.009  $\text{L g}^{-1} \text{cm}^{-1}$ , respectively. It is observed that the  $\alpha_{\text{mass-max}}$  value of the solution of the MDMO-PPV polymer can be increased with decreasing molarity.

The transmittance spectra of the solutions of the MDMO-PPV polymer were taken to investigate their optical properties for 0.261 mM, 6.640 and 3.014  $\mu\text{M}$ , and the plot of the transmittance vs. wavelength is shown in Fig. 4a. As seen in Fig. 4a, the transmittance of the MDMO-PPV polymer increases with decreasing molarity. As seen in Fig. 4a, the transmittance for 0.261 mM sharply increases in the range of about 565 and 615 nm, while the transmittance of the solutions of the MDMO-PPV polymer for 6.640 and 3.014  $\mu\text{M}$  sharply increases in the range of about 520 and 580 nm. In the near ultraviolet and visible region, the average transmittance ( $T_{\text{avg}}$ ) values of the solutions of the MDMO-PPV polymer for 0.261 mM, 6.640 and 3.014  $\mu\text{M}$  were calculated and given in Table 1. As seen in Table 1, the  $T_{\text{avg}}$  values of the MDMO-PPV polymer in the visible region are higher than the values in the near ultraviolet region. As seen in Table 1, the  $T_{\text{avg}}$  values (3.793 and 43.736 %, respectively) of the MDMO-PPV polymer for 0.261 mM in the near ultraviolet and

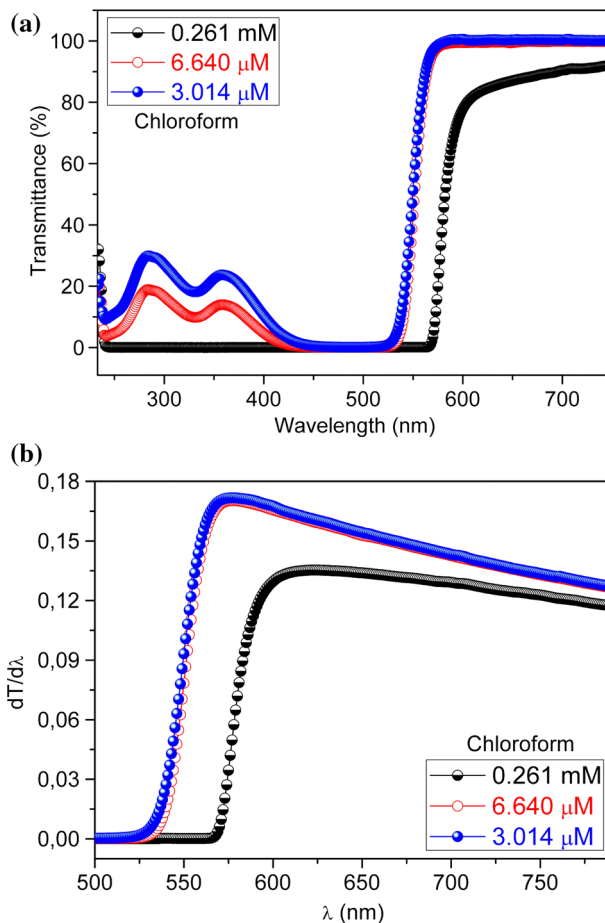


**Fig. 4** **a** The plot of the transmittance vs.  $\lambda$  and **b** the curves of  $dT/d\lambda$  vs.  $\lambda$  of the solutions of the MDMO-PPV polymer for 0.261 mM, 6.640 and 3.014  $\mu\text{M}$  in chloroform solvent



**Table 1** The  $T_{\text{avg-NU}}$  (in the near ultraviolet region),  $T_{\text{avg-V}}$  (in the visible region),  $\lambda_{\text{max. peak}}$ , absorption band edge,  $E_g$ ,  $\lambda_{\text{Tfd}}$  (wavelengths at first decrease of transmittance) and  $E_{\text{Tfd}}$  values of the solutions of the MDMO-PPV for 0.261 mM, 6.640 and 3.014  $\mu\text{M}$ 

Molarity ( $\mu\text{M}$ )	$T_{\text{avg-NU}}$ (%)	$T_{\text{avg-V}}$ (%)	$\lambda_{\text{max. peak}}$ (nm)	Absorption band edge (eV)	$E_g$ (eV)	$\lambda_{\text{Tfd}}$ (nm)	$E_{\text{Tfd}}$ (eV)
261	3.793	43.736	624	1.987	2.024	625	1.984
6.640	12.558	57.379	578	2.145	2.188	580	2.138
3.014	19.969	58.937	577	2.149	2.194	578	2.145

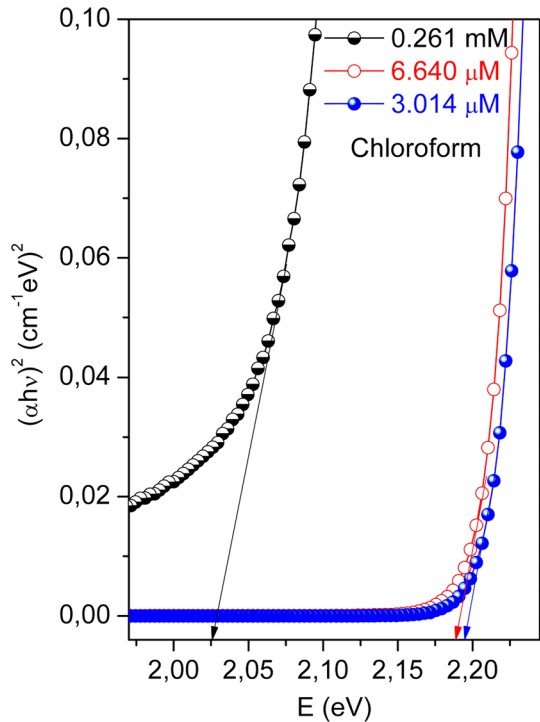
visible region are the lowest values, while the  $T_{\text{avg}}$  values (19.969 and 58.9372 %, respectively) for 3.014  $\mu\text{M}$  are the highest values. It is observed that the average transmittance values of the solutions of the MDMO-PPV polymer in the near ultraviolet and visible region increase with decreasing molarity. To estimate the absorption band edge of the solutions of the MDMO-PPV polymer, the first derivative of the optical transmittance can be computed. For this purpose, the curves of  $dT/d\lambda$  vs.  $\lambda$  of the solutions of the MDMO-PPV polymer for 0.261 mM, 6.640 and 3.014  $\mu\text{M}$  are plotted as shown in Fig. 4b. As seen in Fig. 4b, the maximum peak ( $\lambda_{\text{max}}$ ) position corresponds to the absorption band edge ( $E_{\text{b-e}} = 1240/\lambda_{\text{max}}$ ) and there is a shift in the direction of the higher wavelengths with increasing molarity and the absorption edge of the MDMO-PPV is shifted to higher wavelengths, which is due to the change in the band gap with molarity. In other words, the shifting towards higher wavelengths of the absorption edge is due to decreasing of optical band gap with increasing molarity. The absorption band edge values of the solutions of the MDMO-PPV for 0.261 mM, 6.640 and 3.014  $\mu\text{M}$  were calculated from the maximum peak position and given in Table 1. As seen in Table 1, the maximum peak values of the solutions of the MDMO-PPV polymer vary from 577 to 624 nm. This result suggests that the absorption band edge values of the solutions of the MDMO-PPV polymer shift from 2.149 to 1.987 eV with increasing molarity, that is, the absorption band edge of the solutions of the MDMO-PPV polymer decreases with increasing molarity. The maximum peak values of the MDMO-PPV polymer are higher than the maximum peak value (237 nm) of the parent salicylic acid [33] in the literature, while the absorption band edge values of the MDMO-PPV polymer are lower than the absorption band edge value (5.2 eV) of the parent salicylic acid [33] in the literature.

Optical band gap is a fundamental parameter for electronic, photonic and optoelectronic devices. The optical band gap ( $E_g$ ) of optical transitions can be evaluated from the absorption spectrum and difference between the edges of the valence band and conduction band using the Tauc relation [34, 35]:

$$(\alpha h\nu)^n = C(h\nu - E_g) \quad (3)$$

where  $C$  is a constant,  $h\nu$  is the photon energy ( $E$ ),  $E_g$  is the optical band gap of the material and  $n$  is the parameter measuring type of band gaps. For  $n = 1/2$ ,  $E_g$  in Eq. (3) is direct allowed band gap. To determine the optical band gap of the

**Fig. 5** The  $(\alpha h\nu)^2$  plot vs. the photon energy ( $E$ ) of the MDMO-PPV polymer for 0.261 mM, 6.640 and 3.014  $\mu\text{M}$  in chloroform solvent



solutions of the MDMO-PPV polymer for 0.261 mM, 6.640 and 3.014  $\mu\text{M}$ , the  $(\alpha h\nu)^2$  plot vs.  $E$  of the MDMO-PPV polymer is shown in Fig. 5. As seen in Fig. 5, there is a linear region for the optical band gap of the MDMO-PPV polymer. By extrapolating the linear plot to  $(\alpha h\nu)^2 = 0$  at the linear region, the optical band gap values of the MDMO-PPV polymer were obtained and given in Table 1. As seen in the Table 1, the  $E_g$  value (2.194 eV) of the MDMO-PPV polymer for 3.014  $\mu\text{M}$  is the highest value of all the molarities, while the  $E_g$  value (2.024 eV) of the MDMO-PPV for 0.261 mM is the lowest value. The  $E_g$  values of the MDMO-PPV polymer are in agreement with the value (2.15 eV) for chloroform [25] and are lower than the  $E_g$  value (2.30 eV) of the PEDOT-NB [36] in the literature. This small discrepancy in the band gap of the MDMO-PPV polymer originates from difference of the molarity, process of the coating of the film, form of the material (solution or film) and calculating method of the optical band gap. These results suggest that the optical band gap of the MDMO-PPV polymer can be more decreased with increasing molarity. As seen in Table 1, the obtained  $E_g$  values from the plots of the  $(\alpha h\nu)^2$  vs.  $E$  of the MDMO-PPV polymer are close to values of the first decrease of transmittance of the MDMO-PPV polymer and are close to values of the absorption band edge of the MDMO-PPV polymer. It is observed that the optical band gap of the MDMO-PPV polymer can be found from the plots of  $(\alpha h\nu)^2$  vs.  $E$ , the absorption band edge and the first decrease of transmittance spectra of the MDMO-PPV polymer.

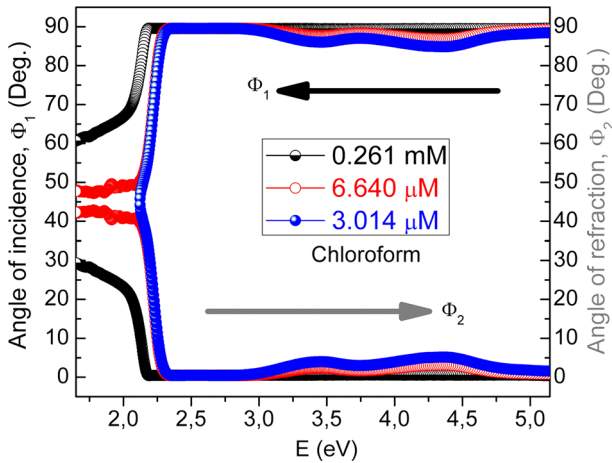


**Fig. 6** The angle ( $\Phi_1$ ) plot of incidence and angle ( $\Phi_2$ ) plot of refraction vs.  $E$  of the solutions of the MDMO-PPV polymer for 0.261 mM, 6.640 and 3.014  $\mu\text{M}$  in chloroform solvent

Incidence angle  $\Phi_1$  is a significant parameter, because voids play important role on electrical, photo-electrical, photovoltaic, photonic, optical, sensing and surface morphology properties of the thin films [37]. The actual solar cell (SC) efficiency should be obtained by accumulating the efficiency over the whole  $\Phi_1$  angle, so the absorption efficiency of the solar cells (SCs) greatly depends on the  $\Phi_1$  angle [37]. Incidence angle  $\Phi_1$  is given as [38–40],

$$\Phi_1 = \tan^{-1} \left( \frac{n_2}{n_1} \right) \tag{4}$$

where  $n_1$  is the refractive index of the medium,  $n_2$  is the refractive index of the solutions of the material. The angle  $\Phi_1$  values of incidence of the solutions of the MDMO-PPV polymer for 0.261 mM, 6.640 and 3.014  $\mu\text{M}$  were calculated from Eq. (4). The  $\Phi_1$  plot vs.  $E$  of the solutions of the MDMO-PPV polymer is shown Fig. 6. As seen in Fig. 6, the angle  $\Phi_1$  values of incidence of the MDMO-PPV polymer increase with increasing photon energy until about 2.38 eV, then they change very little with increasing photon energy and decrease with decreasing molarity. The  $\Phi_1$  values of the MDMO-PPV polymer are close to incidence values of some materials in the literature [41–44]. Similarly, the angle of refraction is calculated from well-known Snell’s law [45]:

$$\Phi_2 = \sin^{-1} \left( \frac{n_1}{n_2} \sin \Phi_1 \right) \tag{5}$$

The angle  $\Phi_2$  values of refraction of the solutions of the MDMO-PPV polymer for 0.261 mM, 6.640 and 3.014  $\mu\text{M}$  were calculated from Eq. (5) and the  $\Phi_2$  plot vs.  $E$  of the MDMO-PPV polymer is shown Fig. 6. As seen in Fig. 6, the angle  $\Phi_2$  values of refraction of the MDMO-PPV decrease sharply with increasing photon

energy until about 2.38 eV, then they change very little with increasing photon energy and increase with decreasing molarity. Similarly, the  $\Phi_2$  values of the MDMO-PPV are close to the  $\Phi_2$  values of some materials in the literature [41, 42, 44]. Also, the angle  $\Phi_1$  values of incidence of the solutions of the MDMO-PPV polymer are higher than the angle  $\Phi_2$  values of refraction. This situation is due to the fact that the refractive index ( $n_2$ ) of the solutions of the MDMO-PPV is higher than the refractive index ( $n_1$ ) of the medium.

The sensitivity of a material is related to a normalized refractive index that is called contrast. The contrast ( $\alpha_c$ ) values of the MDMO-PPV polymer can be calculated by [46];

$$\alpha_c = 1 - \left( \frac{n_1}{n_2} \right)^2 \quad (6)$$

As seen in Fig. 7, the contrasts of the MDMO-PPV polymer for various solvents increase with increasing photon energy and the values of the contrast are higher than 0.60. As seen in Fig. 7, at 1.417 and 2.016 eV, the contrast values (0.745 and 0.950, respectively) for xylene are the highest, while the contrast values (0.609 and 0.790, respectively) for chlorobenzene are the lowest. This result shows that the highest contrast can be obtained with xylene solvent, while the lowest contrast can be obtained with chlorobenzene solvent.

The complex dielectric constant is a very significant parameter to calculate many optical parameters and it is described as [39, 40],

$$\hat{\varepsilon} = \varepsilon_1 + i\varepsilon_2 = \tilde{n}^2 = (n \pm ik)^2 = (n^2 - k^2) + i2nk \quad (7)$$

where  $\varepsilon_1$  is the real part,  $\varepsilon_2$  is the imaginary part of the dielectric constant and  $k = \alpha\lambda/4\pi$ . The  $\varepsilon_1$  and  $\varepsilon_2$  parameters characterize the loss factor. The  $\varepsilon_1$  determines

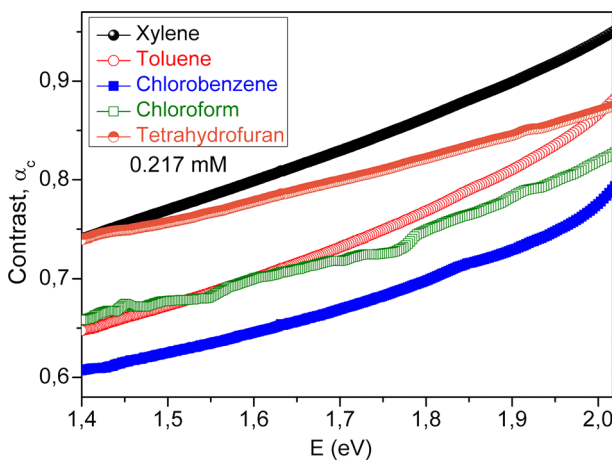


**Fig. 7** The plot of the contrast ( $\alpha_c$ ) vs.  $E$  of the MDMO-PPV polymer for xylene, toluene, chlorobenzene, chloroform and tetrahydrofuran solvents at 0.217 mM

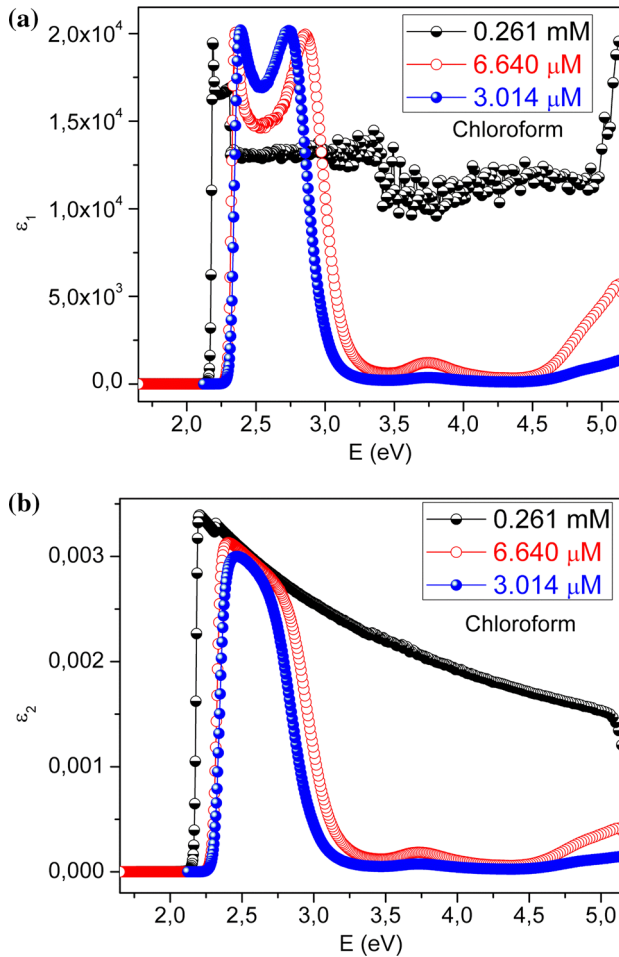


**Fig. 8** The **a** real ( $\epsilon_1$ ) and **b** imaginary ( $\epsilon_2$ ) parts of dielectric constant dependence on photon energy of the MDMO-PPV polymer for 0.261 mM, 6.640 and 3.014  $\mu\text{M}$  in chloroform solvent

the measure by which it will slow down the speed of light in the material and the  $\epsilon_2$  displays the dielectric energy absorbed from an electric field due to dipole motion [47]. Figure 8a, b shows the real and imaginary parts of dielectric constant dependence on photon energy of the MDMO-PPV polymer for 0.261 mM, 6.640 and 3.014  $\mu\text{M}$ , respectively. As seen in Fig. 8a, the real part of dielectric constant of the MDMO-PPV polymer is composed of normal and anomalous (or abnormal) dispersion regions. The  $\epsilon_1$  values of the MDMO-PPV polymer increase with increasing photon energy in normal dispersion region, while the  $\epsilon_1$  values of the MDMO-PPV polymer decrease with increasing photon energy in anomalous (or abnormal) dispersion region. The abnormal (anomalous) behaviors of the MDMO-PPV polymer are due to the resonance effect between the electron polarization and the incident electromagnetic radiation [48], which leads to the coupling of electrons

in solutions of the MDMO-PPV polymer to the oscillating electric field. The  $\varepsilon_1$  values of the MDMO-PPV polymer are higher than the  $\varepsilon_1$  values of the  $\text{Se}_{75}\text{S}_{25-x}\text{Cd}_x$  alloys [49] in the literature. As seen in Fig. 8b, the imaginary part of dielectric constant of the MDMO-PPV polymer decreases with decreasing molarity. The  $\varepsilon_2$  values of the MDMO-PPV polymer are lower than the  $\varepsilon_2$  values of the  $\text{Se}_{75}\text{S}_{25-x}\text{Cd}_x$  alloys [49] in the literature. As seen in Fig. 8a, b, the real part of dielectric constant of the MDMO-PPV polymer is higher than the imaginary part of dielectric constant of the MDMO-PPV polymer.

The optical conductivity ( $\sigma$ ) is one of the most useful tools to investigate the basic properties of materials [50] and it is believed to be a powerful probe in determining electronic characteristics of a variety of materials [51]. The optical properties of the solution of the MDMO-PPV polymer can be analyzed by a complex optical conductivity [39, 40],

$$\sigma(\omega) = \sigma_1(\omega) + i\sigma_2(\omega) \quad (8)$$

where  $\omega = 2\pi f$  is the angular frequency and  $\sigma_1$  is the real part of conductivity and is given as,

$$\sigma_1 = \omega\varepsilon_2\varepsilon_0 \quad (9)$$

and  $\sigma_2$  is the imaginary part of conductivity and is given as,

$$\sigma_2 = \omega\varepsilon_1\varepsilon_0 \quad (10)$$

where  $\varepsilon_0$  is the permittivity of free space. The real part and imaginary parts of the optical conductivity dependence on frequency of the MDMO-PPV polymer for 0.261 mM, 6.640 and 3.014  $\mu\text{M}$  are shown in Fig. 9a, b, respectively. As seen in Fig. 9a, the real part ( $\sigma_1$ ) of the optical conductivity of the MDMO-PPV polymer changes with increasing frequency and decreases with decreasing molarity. As seen in Fig. 9a, the  $\sigma_1$  increases with increasing frequency until about 620 THz. This increase shows that the rate at which electrons absorb the incident photons at a given energy (or frequency) increases [51]. As seen in Fig. 9a, b, the imaginary parts of the optical conductivity of the MDMO-PPV polymer are higher than the real parts of the optical conductivity.

The optical conductivity ( $\sigma_{\text{opt}}$ ) is a measure of the frequency response of the material when irradiated with light and  $\sigma_{\text{opt}}$  can also be calculated as [52, 53],

$$\sigma_{\text{opt}} = \frac{\alpha nc}{4\pi} \quad (11)$$

where  $c$  is the velocity of light. Optical conductivity values of the MDMO-PPV polymer for 0.261 mM, 6.640 and 3.014  $\mu\text{M}$  at 489 nm were found to be  $9.29 \times 10^{11} \text{ s}^{-1}$ ,  $9.21 \times 10^{11} \text{ s}^{-1}$  and  $9.06 \times 10^{11} \text{ s}^{-1}$ , respectively. Optical conductivity values of the MDMO-PPV polymer are higher than the optical conductivity value ( $1.09 \times 10^{10} \text{ s}^{-1}$ ) of the TiN/PVA nanocomposites at 532 nm [47] in the literature.

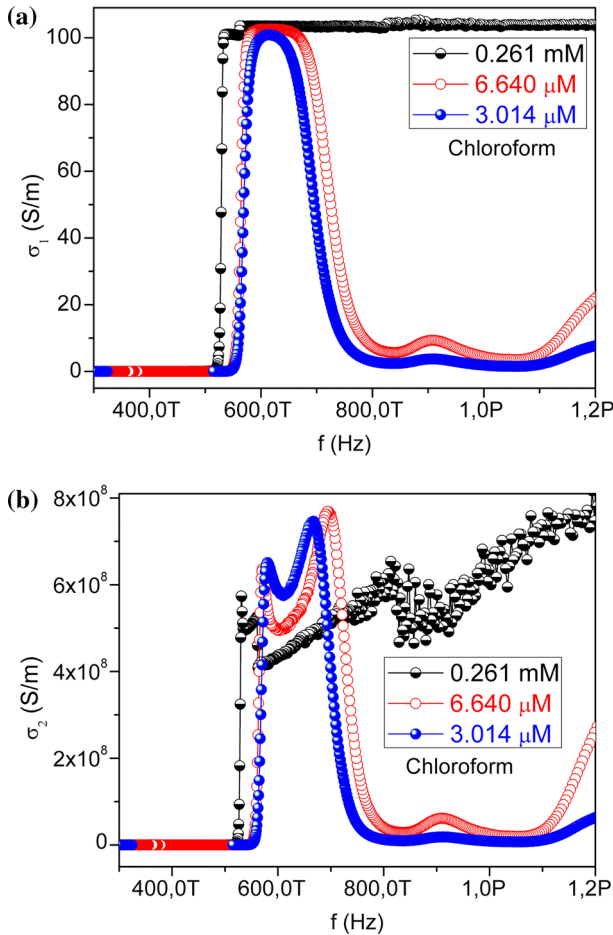


**Fig. 9** The **a** real ( $\sigma_1$ ) and **b** imaginary ( $\sigma_2$ ) parts of the optical conductivity dependence on frequency of the MDMO-PPV polymer for 0.261 mM, 6.640 and 3.014  $\mu$ M in chloroform solvent

**The effects on optical parameters of the MDMO-PPV polymer of the solvents**

To determine the optical band gap  $E_g$  of the solutions of the MDMO-PPV polymer for 0.217 mM of the xylene, toluene, chlorobenzene, chloroform and tetrahydrofuran solvents, the  $(\alpha h\nu)^2$  plot vs. the photon energy  $E$  of the MDMO-PPV polymer is shown in Fig. 10. By extrapolating the linear plot to  $(\alpha h\nu)^2 = 0$  at the linear region, the optical band gap values of the MDMO-PPV polymer were obtained and given in Table 2. As seen in Table 2, the  $E_g$  value (2.103 eV) of the MDMO-PPV polymer for tetrahydrofuran solvent is the highest value, while the  $E_g$  value (2.020 eV) of the MDMO-PPV polymer for xylene solvent is the lowest value. The  $E_g$  values of the MDMO-PPV polymer are in agreement with literature values (2.15, 2.10 and 2.12 eV) [25]. Also, the  $E_g$  values of the solutions of the MDMO-PPV

**Fig. 10** The  $(\alpha h\nu)^2$  plot vs. the photon energy (E) of the MDMO-PPV polymer for xylene, toluene, chlorobenzene, chloroform and tetrahydrofuran solvents at 0.217 mM

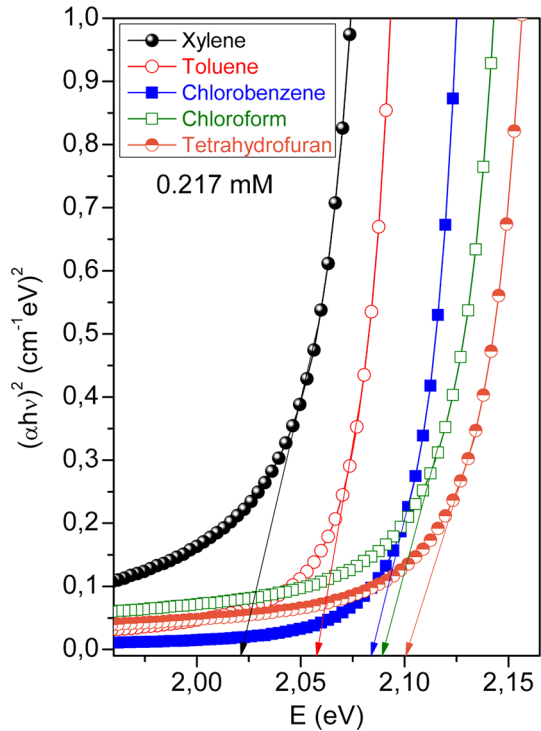


**Table 2** The optical parameters of the MDMO-PPV polymer for xylene, toluene, chlorobenzene, chloroform and tetrahydrofuran solvents

Solvents	Xylene	Toluene	Chlorobenzene	Chloroform	Tetrahydrofuran
$E_g$ (eV)	2.020	2.057	2.083	2.088	2.103
$n$ at 615 nm	4.455	2.882	2.183	2.397	2.823
$n$ at 875 nm	1.981	1.692	1.599	1.723	1.976
$E_0$ (eV)	2.097	2.199	2.402	2.365	2.326
$E_d$ (eV)	3.359	2.406	2.435	2.937	4.241
$M_{-1}$	1.602	1.094	1.014	1.242	1.824
$M_{-3}$ (eV <sup>-2</sup> )	0.364	0.226	0.176	0.222	0.337
$f$ (eV <sup>2</sup> )	7.042	5.291	5.848	6.944	9.862
$n_0$	1.613	1.447	1.419	1.497	1.680
$\chi^{(1)}$	0.128	0.087	0.081	0.099	0.145
$\chi^{(3)}$ (esu) $\times 10^{-13}$	0.510	0.109	0.082	0.183	0.840
$n_2$ (esu) $\times 10^{-12}$	1.191	0.284	0.218	0.461	1.884

polymer are higher than the value (2.36 eV) in the literature [27]. Although the MDMO-PPV polymer was fully dissolved in all the solvents, the lowest optical band gap was obtained for xylene. These results suggest that xylene, toluene, chlorobenzene, chloroform and tetrahydrofuran solvents can be preferred to obtain



lower optical band gap of the MDMO-PPV polymer, respectively. The optical band gap (2.057 eV) of the MDMO-PPV polymer for toluene solvent is lower than the value (2.088) of the MDMO-PPV polymer for chloroform solvent. This result is in agreement with literature values (2.15 eV for chloroform and 2.12 eV for toluene) [25].

Refractive index ( $n$ ) is one of the fundamental properties for an optical material, because it is closely related to the electronic polarizability of ions and the local field inside materials [54, 55], and it is an important parameter for optical, optoelectronic and photovoltaic applications, because high refractive index ( $n$ ) thin film materials (typically  $> 1.65$ ) [56] are generally used to improve the performance of optical and photovoltaic devices in many technologies such as solar cells [41], Bragg gratings [44], photonic crystals [57] and waveguide-based optical circuits [58]. The complex optical refractive index is expressed as,

$$\hat{n} = n(\omega) + ik(\omega) \quad (12)$$

where  $n$  is the real part and  $k$  is the imaginary part of complex refractive index. The optical properties of the MDMO-PPV polymer can be characterized by refractive index. The refractive index is obtained from the following equation [38–40],

$$n = \left\{ \left[ \frac{4R}{(R-1)^2} - k^2 \right]^{1/2} - \frac{R+1}{R-1} \right\} \quad (13)$$

where  $R$  is the reflectance of the MDMO-PPV polymer. The refractive index ( $n$ ) values of the MDMO-PPV polymer for 0.217 mM of the xylene, toluene, chlorobenzene, chloroform and tetrahydrofuran solvents were calculated from Eq. (13). Figure 11a indicates the plot of  $n$  vs.  $\lambda$  of the MDMO-PPV polymer. The refractive index ( $n$ ) values of the MDMO-PPV polymer at 615 and 875 nm are given in Table 2. As seen in Table 2, at 615 nm the  $n$  value (4.455) for xylene is the highest, while the  $n$  value (2.183) for chlorobenzene is the lowest. Similarly, at 875 nm the  $n$  value (1.981) for xylene is the highest, while the  $n$  value (1.599) for chlorobenzene is the lowest. It is observed that the refractive index of the MDMO-PPV polymer decreases with increasing wavelength and the refractive index can be changed with various solvents. The refractive index values of the MDMO-PPV are close to  $n$  values in the literature [41, 43, 44, 54, 59–61].

The refractive index dispersion in semiconductor can be analyzed using the Wemple–Di Domenico (WDD) single oscillator model, which is a semi-empirical relation [39, 40, 62, 63].

$$n^2 - 1 = \frac{E_d E_o}{E_o^2 - E^2} \quad (14)$$

where  $E$  is the photon energy,  $E_o$  is the average excitation energy or single oscillator energy for electronic transitions and  $E_d$  is the dispersion energy, which is a measure of the average strength of inter-band optical transitions or the oscillator strength and is independent of both the absorption band gap and the lattice constants. Experimental verification of Eq. (14) can be obtained by plotting  $(n^2 - 1)^{-1}$

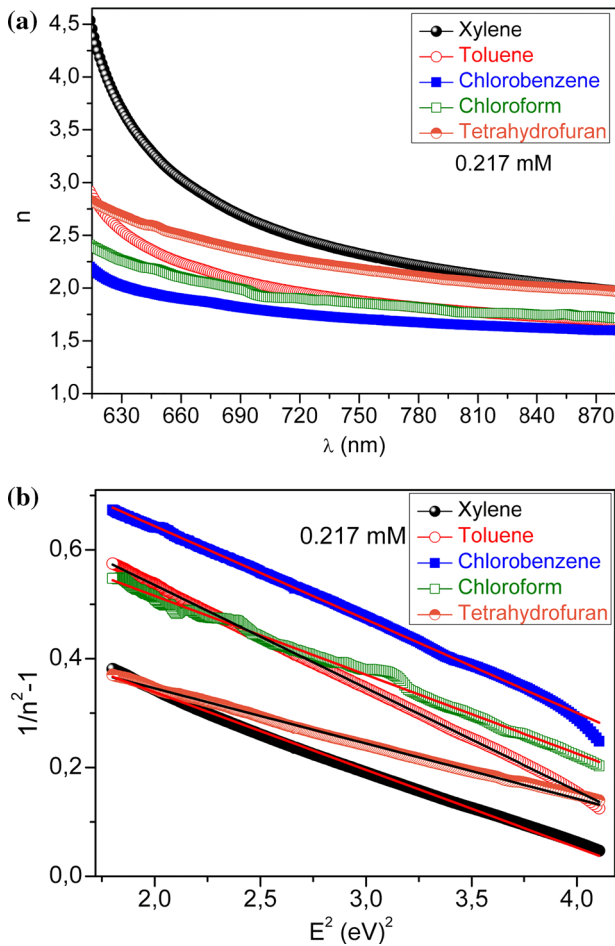


**Fig. 11** **a** The plot of  $n$  vs.  $\lambda$  and **b**  $1/(n^2 - 1)$  vs.  $E^2$  of the MDMO-PPV polymer for xylene, toluene, chlorobenzene, chloroform and tetrahydrofuran solvents at 0.217 mM

vs.  $E^2$ . The plot of the  $1/(n^2 - 1)$  vs.  $E^2$  of the MDMO-PPV polymer is shown in Fig. 11b. The  $E_0$  and  $E_d$  values of the solutions of the MDMO-PPV polymer of the xylene, toluene, chlorobenzene, chloroform and tetrahydrofuran solvents were obtained and given in Table 2. As seen in Table 2, the  $E_d$  value (3.359 eV) is the highest for xylene, while the dispersion energy ( $E_d$ ) value (2.241 eV) is the lowest for tetrahydrofuran solvent. On the other hand, the  $E_0$  value (2.402 eV) is the highest for chlorobenzene, while the single oscillator energy ( $E_0$ ) value (2.097 eV) is the lowest for xylene. The single oscillator energy ( $E_0$ ) values of the MDMO-PPV polymer are lower than the  $E_0$  value (5.5 eV) of the CoPc thin film [64], the  $E_0$  value (3.76 eV) of the  $Y_{0.225}Sr_{0.775}CoO_{3\pm\delta}$  thin film [65] and are higher than  $E_0$  value ( $5.025 \pm 7.1 \times 10^{-5}$  eV) of the  $TlInS_2$  layered single crystal [61] in the literature. Also, the dispersion energy ( $E_d$ ) values of the MDMO-PPV polymer are lower than

the  $E_d$  value (10.0 eV) of the  $Y_{0.225}Sr_{0.775}CoO_{3\pm\delta}$  thin film [65], the  $E_d$  value (14.532 eV) of the CoPc thin film [64] and are higher than  $E_d$  value ( $57.85 \pm 6.7 \times 10^{-5}$  eV) of the  $TlInS_2$  layered single crystal [61]. The  $E_d$  is related to ionicity, anion valency, coordination number, while the  $E_0$  is related to the optical band gap [47].

The moments of the imaginary part of the optical spectrum  $M_{-1}$  and  $M_{-3}$  moments of the MDMO-PPV polymer can be obtained by [65–68]:

$$E_0^2 = \frac{M_{-1}}{M_{-3}} \quad (15)$$

and

$$E_d^2 = \frac{M_{-1}^3}{M_{-3}} \quad (16)$$

The  $M_{-1}$  and  $M_{-3}$  moments of the MDMO-PPV polymer were obtained and given in Table 2. As seen in Table 2, the  $M_{-1}$  value (1.824) is the highest for tetrahydrofuran, while the  $M_{-1}$  moment value (1.014) is the lowest for chlorobenzene. On the other hand, the  $M_{-3}$  value ( $0.364 \text{ eV}^{-2}$ ) is the highest for xylene, while the  $M_{-3}$  moment value ( $0.176 \text{ eV}^{-2}$ ) is the lowest for chlorobenzene.

The optical oscillator strengths ( $f$ ) for optical transitions are considered as absorption of a photon by the electron between the initial state and the final state [65]. The transition rate is proportional to the square ( $f^2$ ) of the oscillator strength. Hence, the oscillator strength may be regarded as an indicator of how strongly the materials interact with the radiation. Hence, the  $f$  is a significant parameter and it is given by the following equation [62]:

$$f = E_0 E_d \quad (17)$$

The oscillator strength ( $f$ ) values of the MDMO-PPV polymer for the xylene, toluene, chlorobenzene, chloroform and tetrahydrofuran solvents were calculated and given in Table 2. As seen in Table 2, the  $f$  value ( $9.862 \text{ eV}^2$ ) is the highest for tetrahydrofuran, while the oscillator strength ( $f$ ) value ( $5.291 \text{ eV}^2$ ) is the lowest for toluene. The oscillator strength ( $f$ ) values of the MDMO-PPV polymer are lower than the oscillator strength value ( $37.51 \text{ eV}^2$ ) of the  $Y_{0.225}Sr_{0.775}CoO_{3\pm\delta}$  thin film [65].

From WDD dispersion parameters  $E_0$  and  $E_d$ , the linear static refractive index ( $n_0$ ) is given using the formula [69, 70]:

$$n_0 = \left(1 + \frac{E_d}{E_0}\right)^{0.5} \quad (18)$$

The  $n_0$  values of the MDMO-PPV for the xylene, toluene, chlorobenzene, chloroform and tetrahydrofuran solvents were calculated and given in Table 2. As seen in Table 2, the  $n_0$  value (1.680) is the highest for tetrahydrofuran, while the  $n_0$  value (1.419) is the lowest for chlorobenzene. The  $n_0$  values of the MDMO-PPV are lower than the  $n_0$  value (1.905) of the TiN/PVA nanocomposites [47] in the literature.

Optical linear susceptibility ( $\chi^{(1)}$ ) is an important parameter and is given by [47]:

$$\chi^{(1)} = \frac{E_d}{4\pi E_0} \quad (19)$$

Optical linear susceptibility ( $\chi^{(1)}$ ) values of the MDMO-PPV for the xylene, toluene, chlorobenzene, chloroform and tetrahydrofuran solvents were calculated and given in Table 2. As seen in Table 2, the  $\chi^{(1)}$  value (0.145) is the highest for tetrahydrofuran, while the  $\chi^{(1)}$  value (0.081) is the lowest for chlorobenzene. The  $\chi^{(1)}$  values of the MDMO-PPV are lower than the  $\chi^{(1)}$  value (0.209) of the TiN/PVA nanocomposites [47] in the literature.

The nonlinear refractive index ( $n_2$ ) and third-order nonlinear susceptibility ( $\chi^{(3)}$ ) parameters are calculated by combining Miller's generalized rule and the relation concerning  $\chi^{(1)}$  and  $\chi^{(3)}$  involving parameters from WDD single oscillator model [70–72]. The  $\chi^{(3)}$  value is given as:

$$\chi^{(3)} = A(\chi^{(1)})^4 \quad (20)$$

Third-order nonlinear susceptibility ( $\chi^{(3)}$ ) values of the MDMO-PPV for the xylene, toluene, chlorobenzene, chloroform and tetrahydrofuran solvents were calculated and given in Table 2. As seen in Table 2, the  $\chi^{(3)}$  value ( $0.840 \times 10^{-13}$  esu) is the highest for tetrahydrofuran, while the  $\chi^{(3)}$  value ( $0.082 \times 10^{-13}$  esu) is the lowest for chlorobenzene. The  $\chi^{(3)}$  values of the MDMO-PPV are lower than the  $\chi^{(3)}$  value ( $3.262 \times 10^{-13}$  esu) of the TiN/PVA nanocomposites [47] in the literature.

Nonlinear refractive index ( $n_2$ ) is related to the third-order susceptibility by:

$$n_2 = \frac{12\pi\chi^{(3)}}{n_0} \quad (21)$$

The nonlinear refractive index ( $n_2$ ) values of the MDMO-PPV for the xylene, toluene, chlorobenzene, chloroform and tetrahydrofuran solvents were calculated and given in Table 2. As seen in Table 2, the  $n_2$  value ( $1.884 \times 10^{-12}$  esu) is the highest for tetrahydrofuran, while the  $n_2$  value ( $0.218 \times 10^{-12}$  esu) is the lowest for chlorobenzene. The  $n_2$  values of the MDMO-PPV are lower than the  $n_2$  value ( $6.454 \times 10^{-12}$  esu) of the TiN/PVA nanocomposites [47] in the literature. The practical relevance of optical susceptibility, nonlinear refractive index and linear static refractive index can be given as:

$$\chi^{(1)} = \left( \frac{n_2 n_0}{12\pi A} \right)^{1/4} \quad (22)$$

Estimated A value was found to be  $1.89 \times 10^{-10}$ . This A value corresponds with A values obtained by Wang [72] for some ionic crystals:  $0.6 \times 10^{-10} < A < 2.5 \times 10^{-10}$ .

## Surface morphology properties of the MDMO-PPV film

Surface morphology properties of the MDMO-PPV film were investigated by high-performance atomic force microscopy. Figure 12a, b shows two (2D)- and three-dimensional (3D) topography images of the MDMO-PPV film for  $5 \times 5 \mu\text{m}^2$  scan area, respectively. As seen in Fig. 12a, b, the topography images have the light and dark regions. The color intensity as seen in Fig. 12a, b shows the vertical profile of the material surface, with light regions being the highest points and the dark points representing the depressions and pores [11].

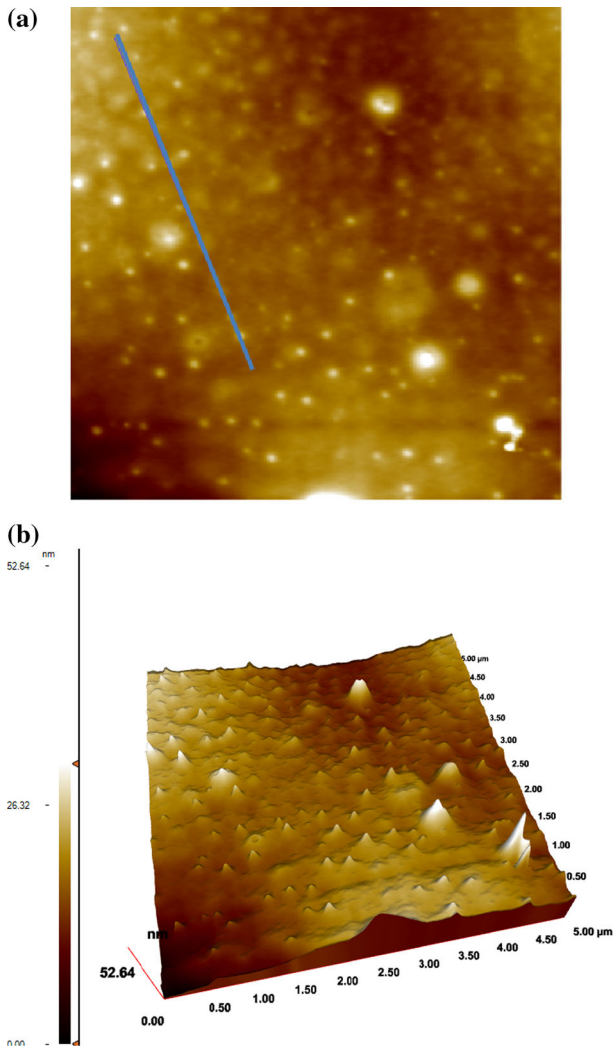


**Fig. 12** a Two (2D)- and b three-dimensional (3D)  $5 \times 5 \mu\text{m}^2$  scan area topography images of AFM of the MDMO-PPV film

There are very significant four types of roughness parameters such as roughness average (Sa), root mean square roughness (Sq), surface skewness (Ssk), and surface kurtosis (Sku). The surface roughness parameters of the MDMO-PPV film such as Sq, Ssk and Sku values were obtained from the AFM images with an AFM software program. The Sa value (2.924 nm) of the MDMO-PPV film is lower than the Sq value (3.793 nm). The Sa value (2.924 nm) of the MDMO-PPV film is lower than the Sa value (6.99 nm) of the MDMO-PPV thin film in the literature [25]. The Sq value of the MDMO-PPV film is lower than the Sq value (5.16 nm) of the PSFP film [73] in the literature. For a Gaussian distribution of asperity height, statistical theory shows that the ratio of Sq to Sa should be 1.25. Ward [74] notes that the asperity height distribution of most engineering surfaces (tribology) may be approximated by a Gaussian distribution with Sq/Sa values of up to 1.31. The ratio (1.297) of the Sq/Sa of the MDMO-PPV film is reasonably close to the value of 1.25 predicted by theory. This result shows that the statistical relationships for surface roughness are applicable [75].

The Ssk value (0.186) of the MDMO-PPV film is positive, the positive value shows that the peaks are dominant on the surface as seen in Fig. 12b. Skewness describes the asymmetry of the height distribution (HD) and is equal to 0 for a Gaussian surface [76]. The surface of the MDMO-PPV film have a simple shape and more advanced parameters are needed to fully describe the surface structure because of the Ssk value (0.186) < 1.5. It is observed that positive skewness values of the MDMO-PPV film predict higher contact force, real area of contact, number of contacting asperities, tangential and adhesion forces than the Gaussian case [77]. It is observed that positive skewness of the MDMO-PPV film results in lower friction coefficient values than the Gaussian case [77]. A positive Ssk value of the MDMO-PPV film indicates a surface with islands and an asymmetry in the height histogram and an additional Gaussian component in the HD [76].

The Sku value (5.328) of the MDMO-PPV film is higher than 3, which indicate the low valleys with spiky surface as seen in Fig. 12a, b. In the literature [75],  $Sku > 3$  for spiky surfaces;  $Sku < 3$  for bumpy surfaces;  $Sku = 3$  for perfectly random surfaces. The Sku value of the MDMO-PPV film shows that the MDMO-PPV film indicates spiky and sharp islands or holes surfaces as seen in Fig. 12a, b. It is known that the rough surfaces with positive skewness and high kurtosis values reduce friction [42, 78]. The positive skewness and high kurtosis values of the MDMO-PPV film are desirable to achieve low friction applications [77]. The distributions with kurtosis values higher than three of the MDMO-PPV film predict higher contact and friction parameters with larger deviations compared to the Gaussian case [77]. The effect of skewness and kurtosis on the static friction coefficient is significant practical engineering field [77]. The effect of kurtosis on the static friction coefficient of the MDMO-PPV film is different, because different trends are observed for kurtosis  $> 3$  [77].

Figure 13a, b shows the histogram and cross-section plots of the MDMO-PPV film for  $5 \times 5 \mu\text{m}^2$  scan area, respectively. The histogram is a graph of neighboring columns. Each column represents a height range. The height of each column represents the number of image pixels, which have a height value in the particular range. As seen in Fig. 13a, all columns have the same width, i.e., they represent the

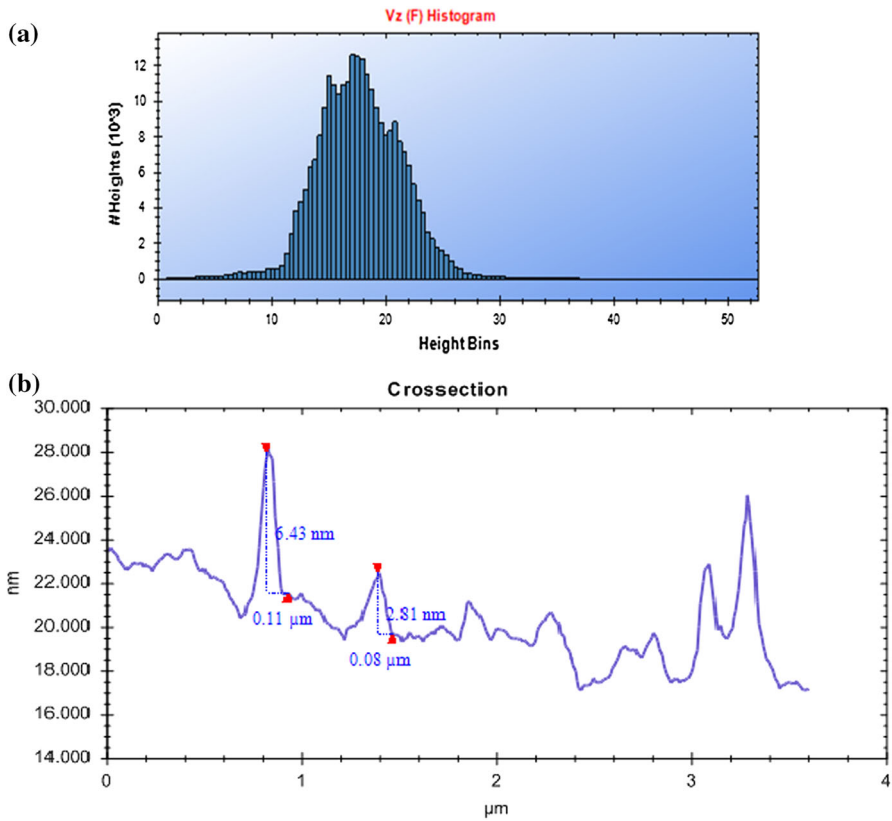


**Fig. 13** **a** The histogram and **b** cross section for  $5 \times 5 \mu\text{m}^2$  scan area plots of the MDMO-PPV film

same height span. As seen in Fig. 13b, the cross-section plot of the MDMO-PPV film was obtained for blue line region in Fig. 12a and it is formed many spiky surfaces as seen in Fig. 13b. As seen in Fig. 13b, the heights of the first and second peaks of the MDMO-PPV film are 6.43 and 2.81 nm, respectively.

## Conclusions

The solution technique in this study is cheaper and more accurate than a film technique to investigate the optical properties of the solutions of the MDMO-PPV polymer. The effects of the molarities on the optical parameters were investigated. The optical band gap of the solution of the MDMO-PPV polymer was decreased with high molarities and various solvents. The orange light of the MDMO-PPV polymer is emitted at about 598 nm for 0.261 mM, while the yellow light of the MDMO-PPV polymer at about 580 nm. The MDMO-PPV exhibited low transmittance values in the visible region, so it can be used in fabrication of some devices such as an image sensor packaging structure and high intensity medium-pressure

lamps. The optical band gap of the MDMO-PPV polymer can be found from the plots of  $(\alpha h\nu)^2$  vs.  $E$ , the absorption band edge and the first decrease of transmittance spectra of the MDMO-PPV polymer. Xylene, toluene, chlorobenzene, chloroform and tetrahydrofuran solvents can be preferred to obtain lower optical band gap values of the MDMO-PPV polymer, respectively. The MDMO-PPV is suitable material for fabrication of the metal–semiconductor (MS) contacts like Schottky diode due to low optical band gap and suitable optical parameters. The ratio (1,297) of the root mean square roughness (Sq) (3.793 nm)/roughness average (Sa) (2.924 nm) of the MDMO-PPV film is close to the value of 1.25 predicted by theory.

**Acknowledgments** This work was supported by The Management Unit of Scientific Research Projects of Muş Alparslan University (MUSBAP) under Project 0001. The author is grateful to Mrs. Hilal Gözler who is R&D Scientist and Nanomagnetic Instruments Co. because of helping with the AFM measurements.

## References

1. Díaz Espinoza MS, Poblete VH, Bernede JC, Cattin L, Godoy A, Díaz Alzamora FR, Gaumer N (2013) Synthesis and optical behavior of PLED devices based on (PMMA)/(PAA)/Er(AP)6Cl3 complex and N, N'-didodecyl-3,4,9,10-perylene tetracarboxylic diimide composites. *Polym Bull* 70 (10):2801–2814
2. Dimitrakopoulos CD, Malenfant PRL (2002) Organic thin film transistors for large area electronics. *Adv Mater* 14:99–117
3. Yildiz HB, Kiralp S, Toppare L, Yilmaz F, Yagci Y, Ito K, Senyo T (2005) Conducting copolymers of 3-methylthienyl methacrylate and p-vinylbenzyloxy poly(ethyleneoxide) and their electrochromic properties. *Polym Bull* 53:193–201
4. Gunduz B, Yahia IS, Yakuphanoglu F (2012) Electrical and photoconductivity properties of p-Si/P3HT/Al and p-Si/P3HT:MEH-PPV/Al organic devices: comparison study. *Microelectron Eng* 98:41–57
5. Ellahi M, Liu F, Song P, Gao Y, Cao H, Rafique MY, Khaskheli MA, Iqbal MZ, Yang H (2013) Influence of the multi-functional epoxy monomers structure on the electro-optical properties and morphology of polymer-dispersed liquid crystal films. *Polym Bull* 70(11):2967–2980
6. Zehetmeyer G, Scheibel JM, Soares RMD, Weibel DE, Oviedo MAS, Oliveira RVB (2013) Morphological, optical, and barrier properties of PP/MMT nanocomposites. *Polym Bull* 70(8):2181–2191
7. Yakuphanoglu F, Gunduz B (2012) Effects of channel widths, thicknesses of active layer on the electrical and photosensing properties of the 6,13-bis(triisopropylsilylethynyl) pentacene transistors by thermal evaporation method: comparison study. *Synth Met* 162:1210–1239
8. Hoppe H, Sariciftci NS (2008) Polymer Solar Cells. *Adv Polym Sci*. 214:1–86
9. Saxena K, Kumar P, Jain VK (2011) Studies on the fluorescence properties of conjugated polymer poly[2-methoxy-5-(3',7'-dimethyloctyloxy)-1,4-phenylenevinylene in presence of nitrogen dioxide gas. *Synth Met* 161:369–372
10. Vishnumurthy KA, Sunitha MS, Adhikari AV (2013) Synthesis and characterization of thiophene-based donor–acceptor type polyimide and polyazomethines for optical limiting applications. *Polym Bull* 70(1):147–169
11. Gizli N (2011) Morphological characterization of cellulose acetate based reverse osmosis membranes by Atomic Force Microscopy (FM) effect of evaporation time. *Chem Chem Technol* 5(3):327–331
12. Nicolescu FA, Jerca VV, Vuluga DM, Vasilescu DS (2010) Synthesis and characterization of side-chain poly(methacrylate)s bearing new azo-moieties. *Polym Bull* 65:905–916
13. Goldys EM, Shi JJ (1998) Linear and nonlinear intersubband optical absorption in a strained double barrier quantum well. *Phys Status Solidi B* 210:237–248
14. Palewicz M, Iwan A, Doskocz J, Strek W, Sek D, Kaczmarczyk B, Mazurek B (2011) Optical and structural study of thin film of polyazomethine with triphenylamine unit prepared via spin-coating method. *Polym Bull* 66:65–76



15. Baghrmryan HM, Barseghyan MG, Kirakosyan AA, Restrepo RL, Duque CA (2013) Linear and nonlinear optical absorption coefficients in GaAs/Ga<sub>1-x</sub>Al<sub>x</sub>As concentric double quantum rings: effects of hydrostatic pressure and aluminum concentration. *J Lumin* 134:594–599
16. Kazarinov RF, Suris RA (1971) Possibility of the amplification of electromagnetic waves in a semiconductor with a superlattice. *Sov Phys Semicond* 5:707–709
17. Miller DAB (1990) Quantum-well optoelectronic switching devices. *Int J High Speed Electron Syst* 1:19–46
18. Hood TH (1988) Multiple quantum well (MQW) waveguide modulators. *J Lightwave Technol* 6:743–757
19. Li Y, Scales N, Blankenship RE, Willows RD, Chen M (2012) Extinction coefficient for red-shifted chlorophylls: chlorophyll d and chlorophyll f. *Biochim Biophys Acta* 1817:1292–1298
20. Beer A (1852) Determination of the absorption of red light in colored liquids. *Ann Phys* 86:78–88
21. Zakerhamidi MS, Ghanadzadeh A, Moghadam M (2012) Solvent effects on the UV/visible absorption spectra of some aminoazobenzene dyes. *Chem Sci Trans.* 1(1):1–8
22. Catalán J, Catalán JP (2011) On the solvatochromism of the  $n \rightarrow \pi^*$  electronic transitions in ketones. *Phys Chem Chem Phys* 13:4072–4082
23. Nesheva DD, Vateva E, Levi Z, Arsova D (2007) Thin film semiconductor nanomaterials and nanostructures prepared by physical vapour deposition: an atomic force microscopy study. *Journal of Physics and Chemistry of Solids* 68:675–680
24. Quist PAC, Martens T, Mancab JV, Savenije TJ, Siebbeles LDA (2006) Photo-induced charge separation and electron diffusion in MDMO-PPV:PCBM bulk heterojunctions. *Sol Energy Mater Sol Cells* 90:362–378
25. Omer BM (2013) Optical properties of MDMO-PPV and MDMO-PPV/[6,6]-phenyl C61-butyric acid 3-ethylthiophene ester thin films. *Int J Organic Electron IJOE* 2(2):1–7
26. Veenstra SC, Verhees WJH, Kroon JM, Koetse MM, Sweelssen J, Bastiaansen JJAM, Schoo HFM, Yang X, Alexeev A, Loos J, Schubert US, Wienk MM (2004) Photovoltaic properties of a conjugated polymer blend of MDMO-PPV and PCNEPV. *Chem Mater* 16:2503–2508
27. Kim S, Ryu S (2010) Efficiency of flexible organic solar cells as a function of post-annealing temperatures. *Curr Appl Phys* 10:e181–e184
28. Saxena K, Kumar P, Jain VK (2010) Fluorescence quenching studies of conjugated polymer poly[2-methoxy-5-(30,70-dimethyloctyloxy)-1,4-phenylenevinylene] in the presence of TNT. *J Lumin* 130:2260–2264
29. Kumar A, Singh S, Mudahar GS, Thind KS (2006) Molar extinction coefficients of some commonly used solvents. *Radiat Phys Chem* 75:737–740
30. Jiang KJ, Xia JB, Masaki N, Noda S, Yanagida S (2008) Efficient sensitization of nanocrystalline TiO<sub>2</sub> films with high molar extinction coefficient ruthenium complex. *Inorg Chim Acta* 361:783–785
31. Zhang H, Fan J, Iqbal Z, Kuang DB, Wang L, Meier H, Cao D (2013) Novel dithieno[3,2-b:2',3'-d] pyrrole-based organic dyes with high molar extinction coefficient for dye-sensitized solar cells. *Org Electron* 14:2071–2081
32. Nunes JK, Ertas M, Du L, DeSimone JM (2010) Hierarchical control of polymer composite nano- and micro-structure with lithography. *Chem Mater* 22:4069–4075
33. Saber O (2012) Improvement of optical properties and thermal stability of poly vinyl alcohol using salicylic acid confined in nanohybrid material. *Polym Bull* 68:209–222
34. Tauc J, Menth A (1972) States in the gap. *J Non-Cryst Solids* 8–10:569–585
35. Stenzel O (2005) The physics of thin film optical spectra: an introduction. Springer-Verlag, Berlin Heidelberg, Germany
36. Abdolmaleki A, Mohamadi Z, Rezaei B, Askarpour N (2013) Synthesis of small-band gap poly(3,4-ethylenedioxythiophene methine)s using acidic ionic liquids as catalyst. *Polym Bull* 70:665–679
37. Lee S, Jeong I, Kim HP, Hwang SY, Kim TJ, Kim YD, Jang J, Kim J (2013) Effect of incidence angle and polarization on the optimized layer structure of organic solar cells. *Sol Energy Mater Sol Cells* 118:9–17
38. Abeles F (1972) Optical properties of solids. North-Holland Publishing Company, London, Amsterdam
39. Turan N, Kaya E, Gündüz B, Çolak N, Körkoca H (2012) Synthesis, characterization of poly(E)-3-amino-4-((3-bromophenyl)diazonyl)-1H-pyrazol-5-ol: investigation of antibacterial activity, fluorescence, and optical properties. *Fibers and Polymers* 13(4):415–424

40. Kaya E, Turan N, Gündüz B, Çolak N, Korkoca H (2012) Synthesis, characterization of poly-2- (2-hydroxybenzylideneamino)-6-phenyl-4,5,6, 7-tetrahydrobenzo[b]thiophene-3-carbonitrile: investigation of antibacterial activity and optical properties. *Polym Eng Sci* 52(7):1581–1589
41. Leguijt C, Lok Igen P, Eikelboom JA, Weeper AW, Schuurmans FM, Sinke WC, Alkemada PFA, Sarro PM, Maree CHM, Verhoef LA (1996) Low temperature surface passivation for silicon solar cells. *Sol Energy Mater Sol Cells* 40:297–345
42. Gündüz B (2013) Effects of molarity and solvents on the optical properties of the solutions of tris[4-(5-dicyanomethylidenemethyl-2-thienyl)phenyl]amine (TDCV-TPA) and structural properties of its film. *Opt Mater* 36:425–436
43. Todorov R, Paneva A, Petkov K (2010) Optical characterization of thin chalcogenide films by multiple-angle-of-incidence ellipsometry. *Thin Solid Films* 518:3280–3288
44. Cusano A, Iadicicco A, Paladino D, Campopiano S, Cutolo A, Giordano M (2007) Micro-structured fiber Bragg gratings. Part II: towards advanced photonic devices. *Optical Fiber Technology* 13:291–301
45. Adachi S (1999) Optical constants of crystalline and amorphous semiconductors. Kluwer Academic Publishers
46. Purniawan A, Pandraud G, Moh TSY, Marthen A, Vakalopoulos KA, French PJ, Sarro PM (2012) Fabrication and optical measurements of a TiO<sub>2</sub>-ALD evanescent waveguide sensor. *Sensors and Actuators A* 188:127–132
47. Divya S, Nampoori VP, Radhakrishnan P, Mujeeb A (2014) Evaluation of nonlinear optical parameters of TiN/PVA nanocomposite e A comparison between semi empirical relation and Z-Scan results. *Curr Appl Phys* 14:93–98
48. Mitschke U, Bäuerle P (2000) The electroluminescence of organic materials. *J Mater Chem* 10:1471–1507
49. Shamshad AK, Al-Hazmi FS, Al-Heniti S, Faidah AS, Al-Ghamdi AA (2010) Effect of cadmium addition on the optical constants of thermally evaporated amorphous Se–S–Cd thin films. *Curr Appl Phys* 10:145–152
50. Mousavi H (2012) Optical conductivity of carbon nanotubes. *Optics Communications* 285:3137–3139
51. Bouarissa N, Gueddim A, Siddiqui SA, Boucenna M, Al-Hajry A (2014) First-principles study of dielectric properties and optical conductivity of Cd<sub>1-x</sub>Mn<sub>x</sub>Te. *Superlattices Microstruct* 72:319–324
52. Abd El-Raheem MM (2007) Optical properties of GeSeTe thin films. *J Phys: Condens Matter* 19 (21):216209–216215
53. Girisun TCS, Dhanuskodi S (2009) Linear and nonlinear optical properties of trithiourea zinc sulphate single crystals. *Cryst Res Technol* 44:1297–1302
54. Mohammed KI, Jasim FM, Azawe MI (2014) Influence of thickness and crystalline structure on thermal and optical properties of ZnO thin films. *Curr Appl Phys* 14:1318–1324
55. Xue SW, Zu XT, Zhou WL, Deng HX, Xiang X, Zhang L, Deng H (2008) Effects of post-thermal annealing on the optical constants of ZnO thin film. *J. Alloys Compd.* 448:21–26
56. Oubaha M, Elmaghrum S, Copperwhite R, Corcoran B, McDonagh C, Gorin A (2012) Optical properties of high refractive index thin films processed at low-temperature. *Opt Mater* 34:1366–1370
57. Kohoutek T, Orava J, Sawada T, Fudouzi H (2011) Inverse opal photonic crystal of chalcogenide glass by solution processing. *J Colloid Interface Sci* 353:454–458
58. Ho WF, Uddin MA, Chan HP (2009) The stability of high refractive index polymer materials for high-density planar optical circuits. *Polym Degrad Stab* 94:158–161
59. Sakr GB, Yahia IS, Fadel M, Fouad SS, Romcevic N (2010) Optical spectroscopy, optical conductivity, dielectric properties and new methods for determining the gap states of CuSe thin films. *J Alloy Compd* 507:557–562
60. Al-Ghamdi AA, Shamshad AK, Al-Heniti S, Al-Agel FA, Zulfeqar M (2011) Annealing and laser irradiation effects on optical constants of Ga<sub>15</sub>Se<sub>85</sub> and Ga<sub>15</sub>Se<sub>83</sub>In<sub>2</sub> chalcogenide thin films. *Curr Appl Phys* 11:315–320
61. El-Nahass MM, Sallam MM, Abd Al-Wahab AHS (2009) Optical and photoelectric properties of TlInS<sub>2</sub> layered single crystals. *Curr Appl Phys* 9:311–316
62. Wemple SH, DiDomenico M (1969) Optical dispersion and the structure of solids. *Phys Rev Lett* 23:1156–1160
63. Wemple SH, DiDomenico M (1971) Behavior of the electronic dielectric constant in covalent and ionic materials. *Phys. Rev. B* 3:1338–1351

64. El-Nahass MM, El-Gohary Z, Soliman HS (2003) Structural and optical studies of thermally evaporated CoPc thin films. *Opt Laser Technol* 35:523–531
65. Ali AI, Son JY, Ammar AH, Abdel Moez A, Kim YS (2013) Optical and dielectric results of  $Y_{0.225}Sr_{0.775}CoO_{3\pm\delta}$  thin films studied by spectroscopic ellipsometry technique. *Results in Physics* 3:167–172
66. Kurt A (2010) Influence of  $AlCl_3$  on the optical properties of new synthesized 3-armed poly(methyl methacrylate) films. *Turk J Chem* 34:67–79
67. Atyia HE (2006) Influence of deposition temperature on the structural and optical properties of  $InSbSe_3$  films. *J Optoelectron Adv Mater* 8:1359–1366
68. Kurt A, Demirelli K (2010) A study on the optical properties of three-armed polystyrene and poly(styrene-*b*-isobutyl methacrylate). *Polym Eng Sci* 2:268–277
69. Tintu R, Saurav K, Sulakshna K, Nampoori VP, Radhakrishnan P, Sheenu T (2010)  $Ge_{28}Se_{60}Sb_{12}/PVA$  composite films for photonic applications. *J. Non-oxide Glasses* 2(4):167–174
70. Ticha H, Tichy L (2002) Semiempirical relation between non-linear susceptibility (refractive index), linear refractive index and optical gap and its application to amorphous chalcogenides. *J. Optoelectron. Adv. Mater.* 4(2):381–386
71. Shanshan S, Janesha D, Craig BA (2010) Influence of annealing conditions on the optical and structural properties of spin-coated  $As_2S_3$  chalcogenide glass thin films. *Opt Express* 18(6):5472–5480
72. Charles CW (1970) Empirical relation between the linear and the third-order nonlinear optical susceptibilities. *Phys. Rev. B* 2:2045–2048
73. Buruiana LI, Avram E, Popa A, Musteata VE, Ioan S (2012) Electrical conductivity and optical properties of a new quaternized polysulfone. *Polym Bull* 68:1641–1661
74. Ward HC (1982) Profile characterization rough surfaces. Longman, London
75. Kumar BR, Rao TS (2012) AFM Studies on surface morphology, topography and texture of nanostructured zinc aluminum oxide thin films. *Digest J Nanomater Biostruct* 7(4):1881–1889
76. Kolanek K, Tallarida M, Karavaev K, Schmeisser D (2010) In situ studies of the atomic layer deposition of thin  $HfO_2$  dielectrics by ultra high vacuum atomic force microscope. *Thin Solid Films* 518:4688–4691
77. Noureddine T, Polycarpou AA (2004) Modeling the effect of skewness and kurtosis on the static friction coefficient of rough surfaces. *Tribol Int* 37:491–505
78. Liu X, Chetwynd G, Gardner JW (1998) Surface characterization of electro-active thin polymeric film bearings. *Int J Machine Tools Manuf* 38(5–6):669–675